Check for updates

Received: 14 March 2024 | Revised: 10 September 2024 | Accepted: 11 September 2024

DOI: 10.1002/dvdy.746

PHENOTYPE REPORT

Developmental Dynamics WILEY

Patterns of early embryogenesis and growth in the olfactory system of chick (*Gallus gallus domesticus*) based on iodine-enhanced micro-computed tomography

Aneila V. C. Hogan | **Donald G. Cerio** | **Gabriel S. Bever**

Center for Functional Anatomy and Evolution, Johns Hopkins University School of Medicine, Baltimore, Maryland, USA

Correspondence
Aneila V. C. Hogan and Gabriel S. Bever, Center for Functional Anatomy and Evolution, Johns Hopkins University School of Medicine, Baltimore, MD, USA.
Email: ahogan@westernu.edu and gbever1@jhmi.edu

Funding information
National Science Foundation Division of Environmental Biology, Grant/Award Number: DEB-1947001

Abstract

Background: The vertebrate olfactory system entails a complex set of neural/support structures that bridge morphogenetic regions. The developmental mechanisms coordinating this bridge remain unclear, even for model organisms such as chick, *Gallus gallus*. Here, we combine previous growth data on the chick olfactory apparatus with new samples targeting its early embryogenesis. The purpose is to illuminate how early developmental dynamics integrate with scaling relationships to produce adult form and, potentially, evolutionary patterns. Olfactory structures, including epithelium, turbinate, nerve, and olfactory bulb, are considered in the context of neighboring nasal and brain structures.

Results: Axonal outgrowth from the olfactory epithelium, which eventually connects receptor neurons with the brain, begins earlier than previously established. This dynamic marks the beginning of a complex pattern of early differential growth wherein the olfactory bulbs scale with positive allometry relative to both brain volume and turbinate area, which in turn scale isometrically with one another.

Conclusions: The mechanisms driving observed patterns of organogenesis and growth remain unclear awaiting experimental evidence. We discuss competing hypotheses, including the possibility that broad-based isometry of olfactory components reflects constraints imposed by high levels of functional/structural integration. Such integration would include the frontonasal prominence having a strong influence on telencephalic patterning.

KEYWORDS
allometry, birds, brain, diceCT, olfactory bulb, turbinates

1 | INTRODUCTION

The nasal placode is a signaling center crucial to formation of the vertebrate nose, brain, and face, with variations in its developmental patterning producing a diversity of phenotypic outcomes.[1–10] The nasal placodes appear as bilateral thickenings of surface ectoderm and give rise to olfactory primordia, including the nascent sensory olfactory epithelium. Differential proliferation of the surrounding facial prominences causes placode invagination into the cephalic mesenchyme and formation of the nasal pits.[8,11] As these pits deepen, coordination

 © 2024 American Association for Anatomy.

between the epithelia, mesenchyme, and chondrogenesis produce a variety of features, including turbinates, olfactory nerve (i. e., cranial nerve I, CN1), and olfactory bulb (OB). These features integrate to form a structural complex where odorant molecules first bind to highly specified receptor neurons in the olfactory epithelium, binding-induced depolarization then sends an electric signal through the neuronal axon (i. e., CN1) to the OB, which then sends a secondary signal to the deep areas of the brain.[12–16]

Accurate perception of odorants relies both on the number and distribution of these neuronal receptors in the olfactory epithelium and on the spatiotemporal dynamics of signal processing within OB and brain. The nature and timing of the connection between the olfactory epithelium and brain likely influences the form of the olfactory system as a whole as it responds to functional adaptations and competition for space in the nose and head.[17–20] Trade-offs may arise from spatial competition to preserve these vital neuronal connections and could include (but are not limited to) turbinate expansion, changes in neuronal distribution across epithelial space, and potential reorganization of neuronal target trajectories within the brain.[21] Questions regarding constraints and subsequent morphological trade-offs may be studied through the growth dynamics of focal structures. Establishing early developmental patterning can shed light on sources of morphological disparity across phylogenies. However, such study of the olfactory system is currently limited by a dearth of growth data, and this problem is particularly acute for birds.

If variation in the olfactory epithelium has some non-neutral selection coefficient, and the epithelium and its supporting framework bear some significant measure of integration, then a correlated pattern of evolution is the expectation.[18,20,22] For example, olfactory gene repertoire sizes (which code for the number of olfactory receptors in the olfactory epithelium) were correlated with OB size.[23–25] This correlation reflects the "one neuron–one receptor" rule,[13] which states that each olfactory neuron expresses only one olfactory receptor and the axons of neurons expressing that receptor type all converge on one locus in the OB.[26] Similarly, as the surface area of the olfactory epithelium increases, so do the turbinates (skeletal elements that scaffold the nasal epithelium) and the OB, at least in animals with greater olfactory acuity.[27,28]

Mechanisms that underlie these morphological associations are yet to be fully determined. Mesenchymal-to-epithelial signaling coregulates the surface area of the olfactory epithelium and turbinate form during development, but it is unclear whether turbinates or epithelia have primacy during their formation.[10,29] Moreover, there are few studies in embryonic or post-hatch ontogeny that consider these morphological relationships in context with the broader olfactory apparatus (i. e., turbinates, CN1, OB, rest of brain). Detailing olfactory morphogenesis in this broader context, even in one taxon, may reveal developmental mechanisms that influence the evolution of variations in olfactory morphology.

The highly conserved nature of the olfactory pathway means that data from chickens are likely meaningful beyond bird, archosaur, or even reptile-specific patterns.[30] Avian model systems are a cornerstone of our understanding of craniofacial morphogenesis in that, among other things, they were the first systems used to track cell morphogenetic movements over 150 years ago.[31] This extensive knowledge base and accessibility, along with the relatively simple structure of the bird olfactory system, create a useful platform for exploring its morphogenesis and differentiation.

Mechanisms dictating the maturation of the olfactory system are poorly known, even though some elements of the cellular and molecular dialogue underlying olfactory patterning are detailed.[6,10] Much of this effort concentrates on early placodal specification, with few studies considering the morphology of the olfactory system and its associated parts across larger windows of ontogeny. A recent work considered this development across a broad swath of chicken ontogeny (ED5-adult),[21] but early developmental stages that encompass the primary window of olfactory morphogenesis were not included. The present study samples from this small but significant gap to clarify the quantitative and qualitative nature of connections between olfactory placodal derivatives and the central nervous system.

Our two primary goals here are to quantify the growth of the olfactory system and generate new data that clarify how differences in morphogenetic timing partition the nasal cavity and associated olfactory system. We pose the following questions to explore the developing olfactory system: (1) What are the primary windows of turbinate and olfactory morphogenesis in chickens, and how and when do these structures diverge in growth from neighboring organs? (2) What are the scaling relationships between the turbinates, OB, and cerebrum across embryonic development? We describe the developing anatomy of these structures, paying close attention to the path of CN1, budding of the OB, and changing shape of the turbinates. Finally, we predict that OB and olfactory turbinate grow isometrically in pre-hatch development, as in full ontogeny.[21] The alternate hypothesis is that the OB grows allometrically with respect to the turbinates.

10970177, 0, Downloaded from https://anatomypubs.onlinelibrary.wiley.com/doi/10.1002/dvdy.746 by Gabriel Bever - Johns Hopkins University , Wiley Online Library on [30/09/2024]. See the Terms and Conditions (https://onlinelibrary.wiley.com/terms-and-conditions) on Wiley Online Library for rules of use; OA articles are governed by the applicable Creative Commons License

2 | RESULTS

In the following sections, we present the results of our enhanced-contrast CT study and our quantitative assessment of scaling relationships among olfactory structures and neighboring organs. Raw growth trajectories are visualized in Figure 1, and relative sizes of focal structures (measured as ratios) may be referred to in Figure 2.

2.1 | Morphology and Growth

2.1.1 | HH19

The olfactory pits are already present as dimpled impressions of the nasal placode. The pits are flanked medially by the frontonasal mass and laterally by the lateral nasal prominences. The pits appear as small cups in cross-section, the apices of which are almost in contact with the telencephalon (Figure 3B). Developing olfactory nerves are present as they migrate toward the forebrain, but no clear contact is made with the brain. The forebrain is smooth, with no evidence of OB.

2.1.2 | HH24

Nascent OB are present. CN1 contacts the forebrain running ventrolaterally. The nerve runs from nasal placode to rostral telencephalon, where it sits in a furrow of the brain, and from there to OB (Figure 3F). Olfactory pits invaginate more deeply into head mesenchyme. Neuronal thickening of nasal placode is present. The OB protrudes from the telencephalon surface, with an indentation marking the border between cerebrum and OB.

2.1.3 | HH26-27

OB increase in volume by 34% and become increasingly distinct from the rest of the brain (Table 1; Figure 3I). CN1 still runs ventrolaterally in a furrow on the forebrain toward the olfactory pits. Olfactory pits remain open tubes with smooth walls, with no sign of turbinate growth. Pits invaginate further and are thus long and digit-like in cross section (Figure 3H). Walls of the nasal pits are uniformly thick but are more radiopaque around the deepest points of the pits, where axonal formation is occurring. Craniofacial fusion is underway, in that the most-rostral portion of frontonasal mass is in contact with maxillary prominence.

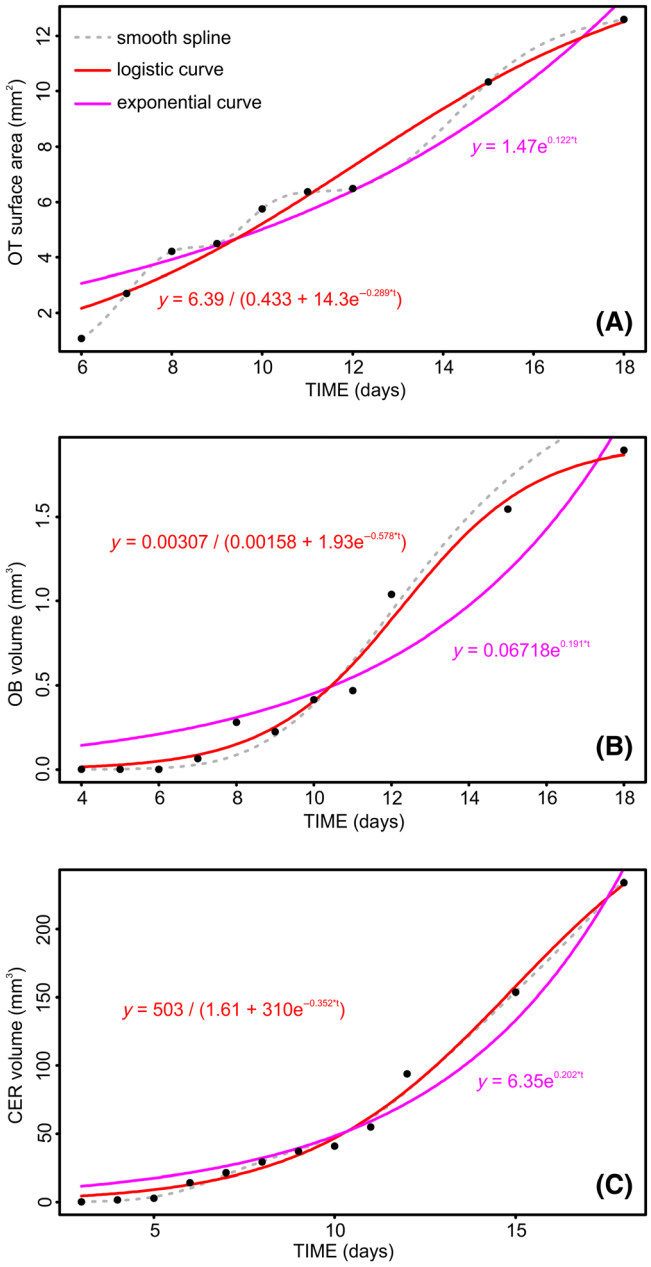

FIGURE 1 Growth of olfactory turbinates (A), olfactory bulb (B), and cerebrum (C) over time (measured in days). A simple smoothed spline, logistic curve (red), and exponential curve (magenta) are fitted to the data, with best-fit equations for the latter curves noted in the appropriate color. CER, cerebrum; OB, olfactory bulb; OT, olfactory turbinate.

2.1.4 | HH29

Fusion of the rostral nasal cavity with craniofacial prominences leaves an epithelial seam (i. e., nasal fin) between maxillary prominence and globular process of frontonasal mass. OB are little changed from preceding stage. Olfactory nerve (CN1) courses ventrally in nearly a straight line toward developing olfactory turbinates (Figure 3M).

10970177, 0, Downloaded from https://anatomypubs.onlinelibrary.wiley.com/doi/10.1002/dvdy.746 by Gabriel Bever - Johns Hopkins University , Wiley Online Library on [30/09/2024]. See the Terms and Conditions (https://onlinelibrary.wiley.com/terms-and-conditions) on Wiley Online Library for rules of use; OA articles are governed by the applicable Creative Commons License

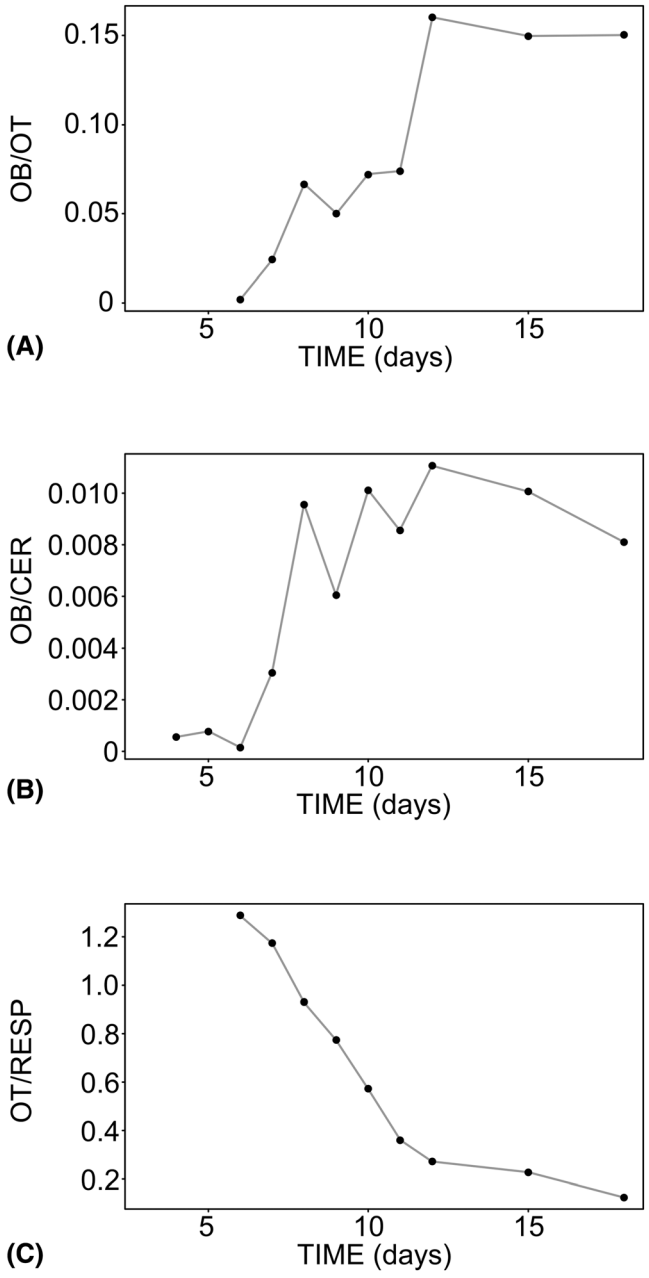

FIGURE 2 Selected growth plots showing changes in volume and surface area ratios between structures during embryonic development. (A) The ratio of olfactory bulb volume (OB) to olfactory turbinate surface area (OT) appears linear with respect to time but with deviations on days 8 and 12. (B) The ratio of cerebrum volume (CER) to OB may or may not be linear with respect to time, and structure size seems to have high variance in this sample. (C) The ratio of OT to respiratory turbinates appears linear with respect to time. CER, cerebrum; OB, olfactory bulb; OT, olfactory turbinate; Resp, respiratory.

The length of CN1 runs apart from forebrain, a considerable change from HH26-27. Nasal pits begin to close, and olfactory and middle turbinates begin to bud from lateral nasal prominences, with the olfactory bud being the thicker of the two. Sensory epithelium covering developing olfactory turbinate is bright white in diceCT data because neural tissues tend to take up iodine stain well. In contrast, non-sensory, respiratory epithelium of middle turbinate, which is directly ventral to sensory epithelium, stains poorly. A transition from well-stained sensory epithelium to poorly stained respiratory epithelium is visible in diceCT data.

2.1.5 | HH31

OB increase in volume by 25% (Table 1). The bulbs are now more piriform in shape and protrude rostrally from cerebrum (Figure 4E). CN1 projects forward from rostralmost aspect of OB at 90° angle from forebrain. The nerve arcs as it courses rostrally to the olfactory turbinates (Figure 4E). Olfactory turbinates increase in surface area dramatically (152%), due partially to medial expansion into nasal cavity (Table 1; Figure 4B,D). Middle turbinates grow by 94%, expanding rostrocaudally just ventral to the olfactory turbinates (Table 1; Figure 4B,D,E). Vestibular turbinates make their first appearance as small projections from dorsal wall of vestibule. Nasal passage is almost entirely closed due to fusion across craniofacial prominences and formation of nasal plug.[32] A caudal space in the nasal passage, just above the choana, remains patent.

2.1.6 | HH34

OB grow 327% in volume (Table 1; Figures 1, 2) and now exhibit the pyramidal shape conserved at perinatal stages (Figure 4J). Junction of OB and cerebrum marked by distinct crease. Rostral arc describing path of CN1 to olfactory turbinates is less pronounced. Olfactory turbinates increase in curvature and surface area (Table 1; Figure 4K,L). Middle turbinates increase in coiling to a 180° scroll. These turbinates also expand rostrocaudally and now extend beyond rostral extent of the olfactory turbinates. Middle turbinates experience most pronounced period of surface-area growth, increasing by 119%. Vestibular turbinates expand rostrally, forming a simple ridge that extends ventrally from dorsal wall of vestibule (Figure 4J,K,L). Surface area of vestibular turbinates increases modestly, by 45%. Nasal passage remains occluded to the choanal opening.

2.1.7 | HH35

Growth slows across nasal and olfactory structures, except for vestibular turbinate, which increases in surface area by 60% (Table 1). Olfactory and middle turbinates

10970177, 0, Downloaded from https://anatomypubs.onlinelibrary.wiley.com/doi/10.1002/dvdy.746 by Gabriel Bever - Johns Hopkins University , Wiley Online Library on [30/09/2024]. See the Terms and Conditions (https://onlinelibrary.wiley.com/terms-and-conditions) on Wiley Online Library for rules of use; OA articles are governed by the applicable Creative Commons License

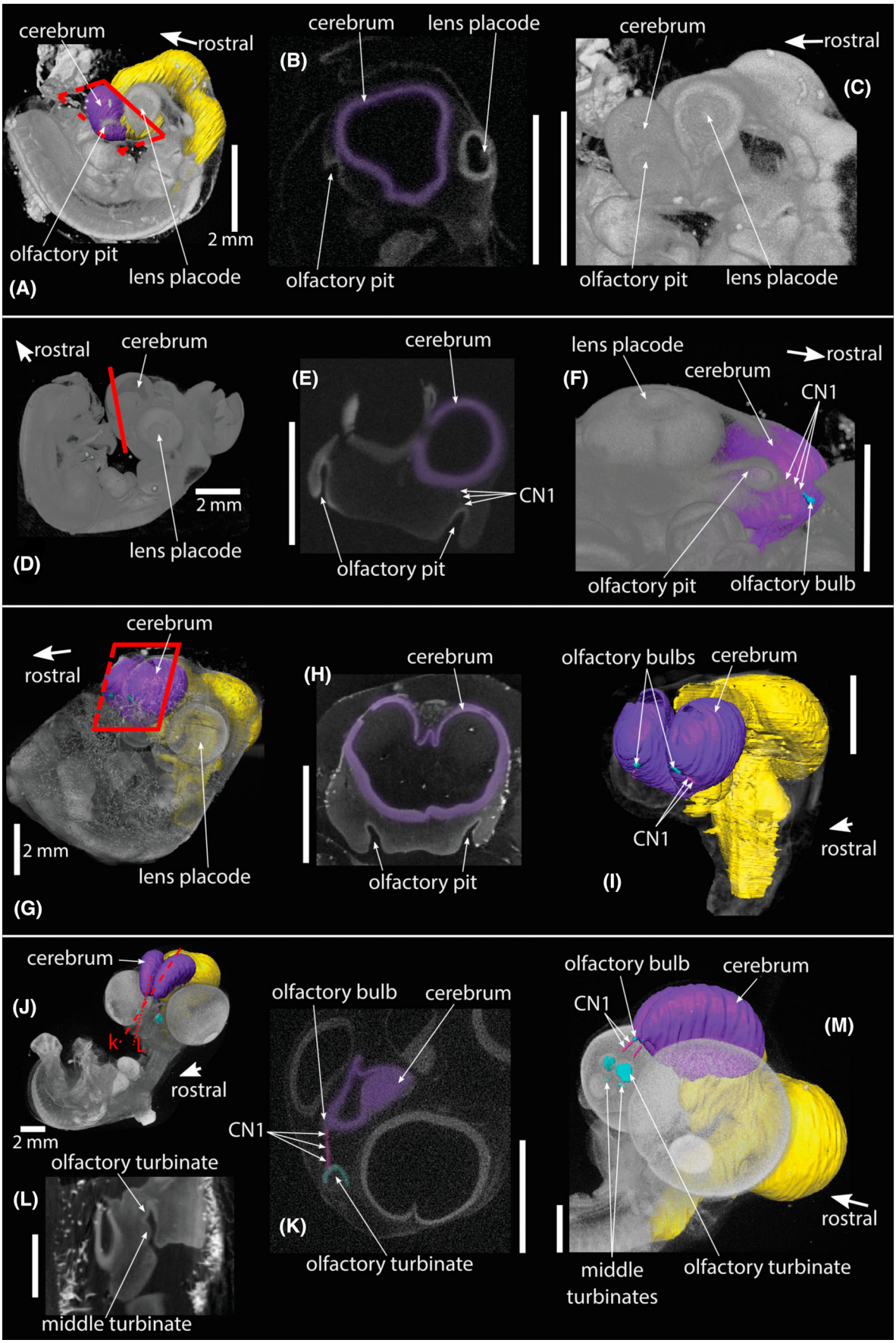

FIGURE 3 Legend on next page.

10970177, 0, Downloaded from https://anatomypubs.onlinelibrary.wiley.com/doi/10.1002/dvdy.746 by Gabriel Bever - Johns Hopkins University , Wiley Online Library on [30/09/2024]. See the Terms and Conditions (https://onlinelibrary.wiley.com/terms-and-conditions) on Wiley Online Library for rules of use; OA articles are governed by the applicable Creative Commons License

TABLE 1 Growth rates and percent increases over time. For growth rates by Hamburger-Hamilton stage, see Data S1 (Table S2).

Time	OB		Cerebrum		Olf turb		Mid turb		Vest turb		Atrial turb	
Days	Rate	%	Rate	%	Rate	%	Rate	%	Rate	%	Rate	%
3–4	—	—	1.59	741	—	—	—	—	—	—	—	—
4–5	$4.8{\cdot}10^{-6}$	34	0.99	55	—	—	—	—	—	—	—	—
5–6	$-6.0{\cdot}10^{-5}$	−2	11.4	401	—	—	—	—	—	—	—	—
6–7	0.063	25	7.25	51	1.63	152	0.78	94	—	—	—	—
7–8	0.214	327	7.82	36	1.51	56	1.91	119	0.31	45	—	—
8–9	−0.070	−25	7.93	27	0.28	6	0.56	16	0.60	60	—	—
9–10	0.200	95	3.79	10	1.26	28	0.46	11	2.97	186	0.80	615
10–11	0.060	15	13.9	34	0.62	10	4.61	101	3.03	66	0.04	4
11–12	0.570	121	38.9	71	0.12	16	4.45	48	1.17	15	0.60	62
12–15	0.170	49	20.0	64	1.28	60	3.22	71	2.57	88	1.28	244
15–18	0.110	18	26.7	52	0.77	22	7.40	96	8.40	153	3.08	171

Abbreviations: Mid, middle; OB, olfactory bulb; Olf, olfactory; Turb, turbinates; Vest, vestibular.

increase only 6% and 16% in surface area, respectively. OB is similar in size across three of four specimens at HH34-35. Specimen 8a (staged at HH34) has OB larger than either 9a or 9b. Stage-mean bulb size thus seems to shrink over 24 h from HH34 to HH35 (Table 1). However, it is more likely OB experiences deceleration or stasis of growth that is also evident in other structures, like olfactory turbinates (Table 1), during this period. Vestibular turbinates expand and begin to scroll (Figure 4N). Atrial turbinate first appears, budding from lateral wall of vestibule into void created by concavity of vestibular turbinates (Figure 4N,O).

2.1.8 | HH36

OB take on a more mature, piriform shape. The OB-cerebral junction has become more constricted (Figure 4U). OB volume increases 95% (Table 1). CN1 arcs 90° from OB to olfactory turbinates (Figure 4U). These turbinates expand rostrocaudally and dorsoventrally (Figure 4U,V,W), though surface area increases only 28%. Middle turbinates modestly increase in scrolling, and surface area increases by only 11% (Figure 4T). Growth is concentrated rostrally, where vestibular turbinates experience their greatest surface area increase of 186%. Vestibular turbinates transform from simple ridge to partially scrolled surface extending ventrally into the vestibule (Figure 4U,V,W). In cross-section, vestibular turbinates are sickle-shaped. This curved nature produces a lateral space between the turbinates and lateral wall of the nasal cavity. Atrial turbinates expand to occupy this space (Figure 4U,V,W). Though external nares remain plugged, nasal passage recanalization is evident between middle turbinates and choanal opening (Figure 4T). Nasal passage is patent adjacent to olfactory turbinates. Nasal plug persists rostrally within olfactory chamber, and nasal passage remains occluded at level of respiratory turbinates.

2.1.9 | HH37

Growth in olfactory structures slows. OB increase in volume by 15% and their form is largely unchanged except that left and right bulbs migrate to midline, forming contralateral contact that persists to maturity. Similarly, left and right CN1 meet near their caudal intersection with OB (Figure 5E). Olfactory turbinates grow medially but little

FIGURE 3 Images from diceCT data of developing brain and peripheral olfactory system from embryonic stages HH19-29 of chick *Gallus gallus*. (A, D, G, J) 3-D reconstructions of specimens at stage HH19 (A), HH24 (D), HH27 (G), and HH29 (J). Red lines and parallelograms indicate planes of cross-sectional images. (B, E, H, L, K) Cross-sectional images whose planes are illustrated in the preceding. Note the changing depth of the olfactory pit and its connectivity with CN1. (C, F, I, M) Magnified views of brain and peripheral olfactory system. Note the changing course of CN1 relative to cerebrum. AT, atrial turbinate; diceCT, diffusible iodine-based contrast-enhanced microCT; HH, Hamburger Hamilton; MT, middle turbinate; OT, olfactory turbinate; VT, vestibular turbinate.

10970177, 0, Downloaded from https://anatomypubs.onlinelibrary.wiley.com/doi/10.1002/dvdy.746 by Gabriel Bever - Johns Hopkins University , Wiley Online Library on [30/09/2024]. See the Terms and Conditions (https://onlinelibrary.wiley.com/terms-and-conditions) on Wiley Online Library for rules of use; OA articles are governed by the applicable Creative Commons License

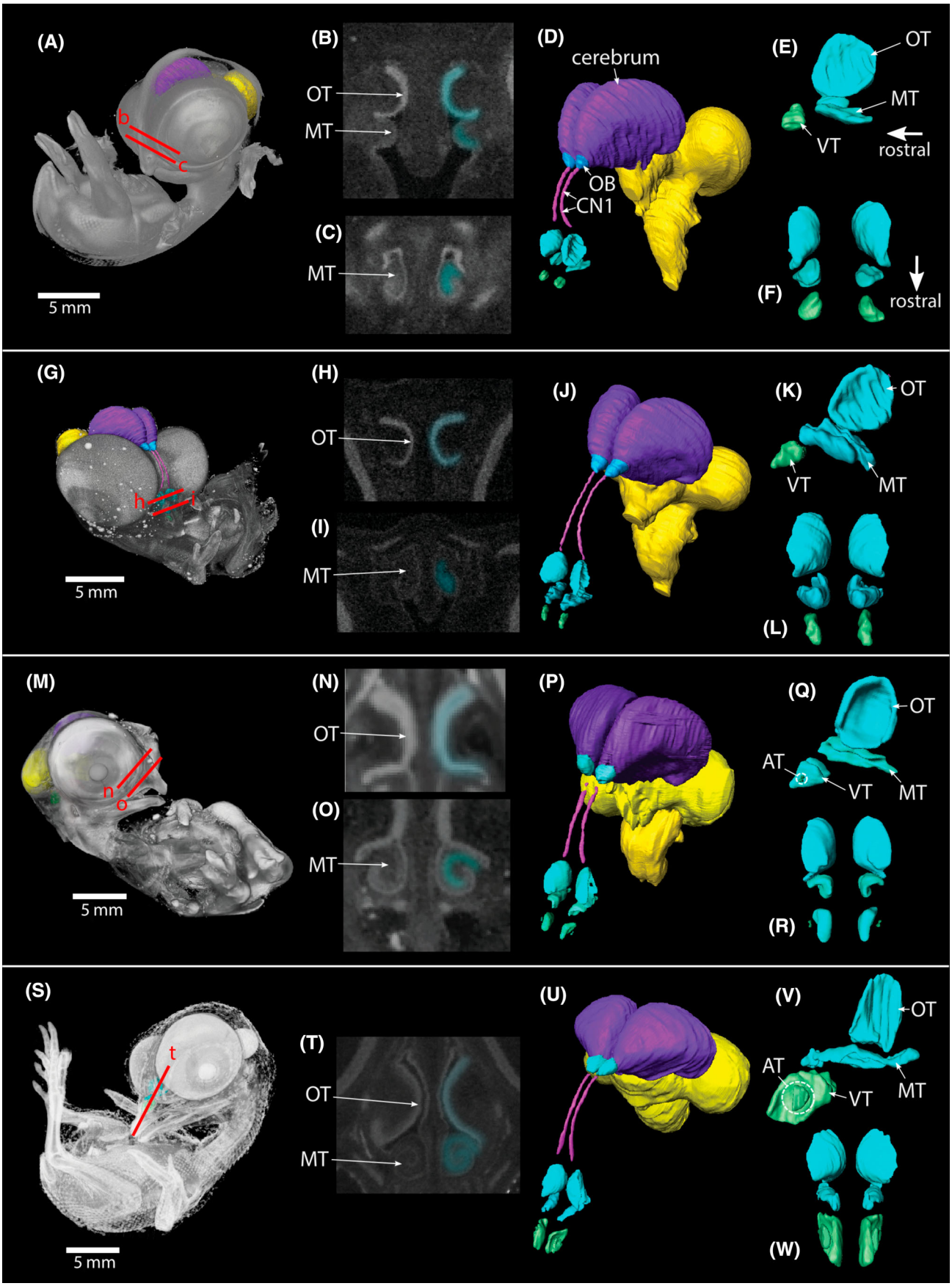

FIGURE 4 Legend on next page.

10970177, 0, Downloaded from https://anatomypubs.onlinelibrary.wiley.com/doi/10.1002/dvdy.746 by Gabriel Bever - Johns Hopkins University , Wiley Online Library on [30/09/2024]. See the Terms and Conditions (https://onlinelibrary.wiley.com/terms-and-conditions) on Wiley Online Library for rules of use; OA articles are governed by the applicable Creative Commons License

rostrocaudally (Figure 5B,D). These turbinates increase in surface area by 10% (Table 1). Respiratory turbinates grow faster. Specifically, middle turbinates now stretch well beyond rostral and caudal extent of the more dorsal olfactory turbinates (Figure 5D). Middle turbinates increase in surface area by 101% and now exceed all other turbinates in size (Figure 5D). These turbinates reach their mature shape of a 360° scroll. Also reaching their mature shape are the vestibular turbinates, which are now falcate in cross-section. These turbinates increase in surface area by 66%. Atrial turbinates increase in surface area by only 4%. Nasal vestibule remains plugged, but middle and olfactory turbinates show advanced recanalization, with nasal passage nearly completely patent near midpoint of middle turbinates (Figure 5B,C).

2.1.10 | HH38

OB increases in volume by 121%, its second-largest increase in the series (Table 1; Figures 1, 2). The bulb retains piriform shape and constriction at intersection with cerebrum (Figure 5J). Middle turbinates increase in surface area by 48% and now scroll approximately 405°. These turbinates still outpace all other turbinates in growth and absolute size (Figure 5I). Curvature of vestibular turbinates is slightly increased, and surface area increases by just 15% (Figure 5I). Atrial turbinates continue to expand, growing medially into vestibular cavity and increasing in surface area by 62% (Figure 5I).

2.1.11 | HH41

OB expand in volume 49% (Table 1). Rostral apices of OB are more rounded, though entire structure remains piriform (Figure 5P). The right and left OB migrated medially and appear nearly contiguous across sagittal midline. Olfactory turbinate increases in surface area by 60% and closely resembles its mature shape (Figure 5N,P,R). Middle and vestibular turbinates increase in surface area by 71% and 88%, respectively. Canalization of nasal passage continues with vestibule remaining plugged. Atrial turbinates expand in surface area by 244% and now nearly fill the lateral recess of the vestibular turbinates (Table 1; Figure 5P, R). Middle turbinates are incompletely patent. In cross section, a narrow arc of radiolucency (about 80% of the turbinates' scroll; Figure 5O) exists between nasal plug and nasal walls. Deepest parts of middle turbinates (i. e., at center of each scroll) remain obstructed by nasal plug.

2.1.12 | HH44

Nearly all structures appear mature. OB growth abates, increasing just 18% in volume. OB form is essentially unchanged. Surface area of olfactory turbinates increases by only 22%. Indeed, most growth occurs in vestibule. Vestibular and middle turbinates increase by 153% and 96%, respectively (Table 1). Atrial turbinate increases in surface area by 171%. Vestibular and atrial turbinates both scroll to about 90° (Figure 5U,X). Atrial turbinates largely fill concavity of vestibular turbinates. Recanalization of nasal canal is nearly complete. Olfactory and middle turbinate sections are completely patent (Figure 5T,U). Only small sections of vestibule, including rostralmost elements of atrial turbinates, remain occluded.

2.2 | Regression analyses

2.2.1 | Embryonic series (HH19–HH44)

OB and olfactory turbinate exhibit allometric growth ($p = <0.0001$, slope = 0.38, 95% CI: 0.26, 0.43) in this early window of development before hatching (Table 2, Figure 6). OB also grow allometrically with other brain regions, which agrees with previous work.[21,33] Regression of cerebrum and OB returns a slope of 1.84 ($p = <0.0001$, 95% CI: 1.4, 2.24). Olfactory turbinate grows isometrically with cerebrum ($p = 0.41$, slope = 0.73, 95% CI: 0.53, 0.92). To sum, OB and its adjacent structures grow with allometry, as do all pairings of turbinates; only a few pairs of focal structures exhibit isometric growth in bivariate comparisons (Figure S1).

FIGURE 4 Images from diceCT data of developing brain and peripheral olfactory system from embryonic stages HH31–36 of chick *Gallus gallus*. (A, G, M, S) 3-D reconstructions of specimens at stage HH31 (A), HH34 (G), HH35 (M), and HH36 (S). Red lines indicate planes of cross-sectional images. (B, C, H, I, N, O, T) Cross-sectional images whose planes are illustrated in the preceding. Note the heavily stained sensory epithelium of olfactory turbinates (OT) that is more radiopaque than the epithelium overlying the respiratory turbinates (AT, MT, VT). (D, J, P, U) Magnified left rostrolateral views of brain and peripheral olfactory system. (E, K, Q, V) Magnified left lateral (top) views of turbinate structures. Note atrial turbinates (AT) developing in the lateral recess of the vestibular turbinates (VT). (F, L, R, W) Magnified rostrodorsal views of turbinate structures. AT, atrial turbinate; CN1, olfactory n.; diceCT, diffusible iodine-based contrast-enhanced microCT; HH, Hamburger Hamilton; MT, middle turbinate; OB, olfactory bulb; OT, olfactory turbinate; VT, vestibular turbinate.

10970177, 0, Downloaded from https://anatomypubs.onlinelibrary.wiley.com/doi/10.1002/dvdy.746 by Gabriel Bever - Johns Hopkins University , Wiley Online Library on [30/09/2024]. See the Terms and Conditions (https://onlinelibrary.wiley.com/terms-and-conditions) on Wiley Online Library for rules of use; OA articles are governed by the applicable Creative Commons License

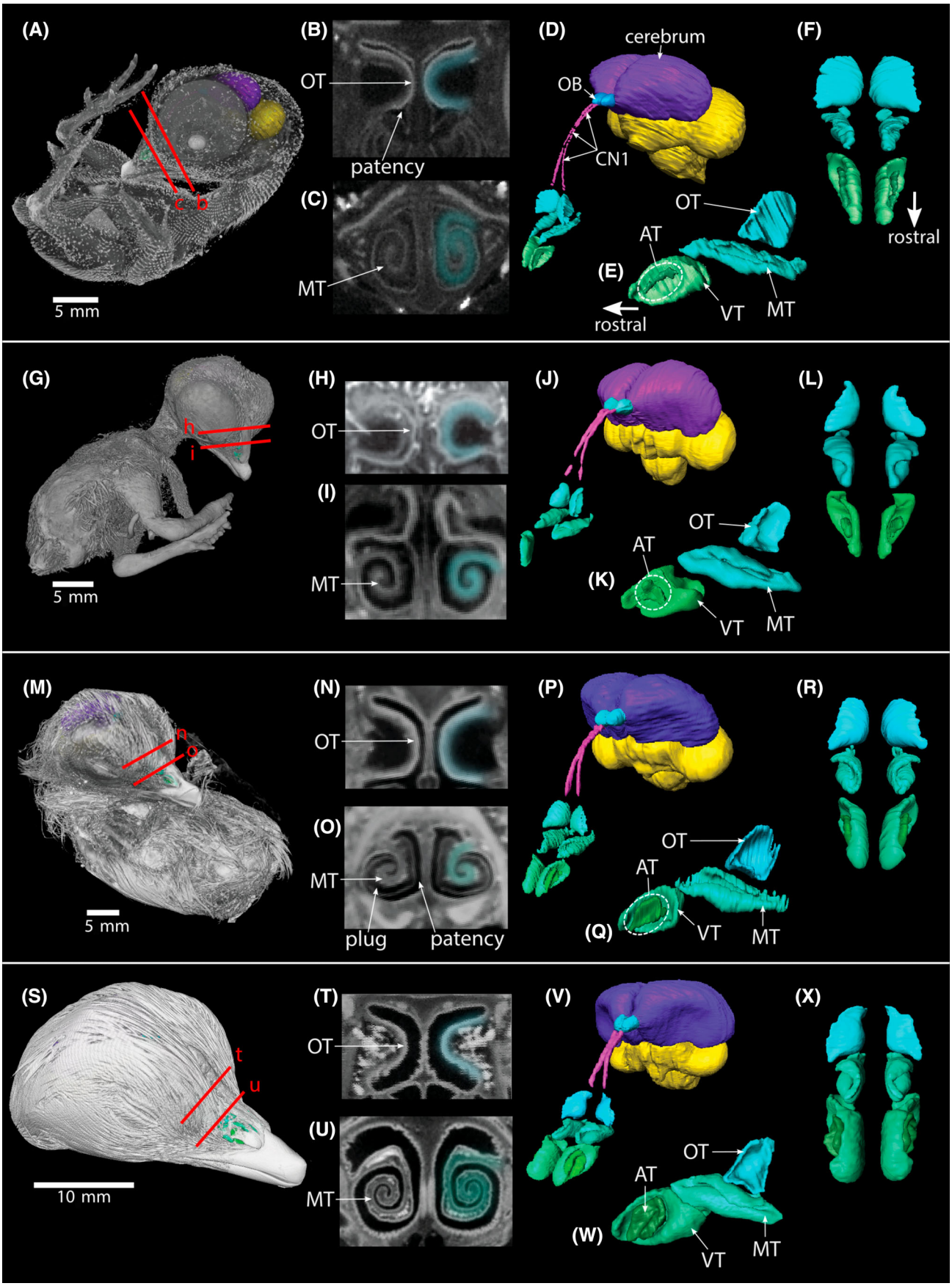

FIGURE 5 Legend on next page.

10970177, 0, Downloaded from https://anatomypubs.onlinelibrary.wiley.com/doi/10.1002/dvdy.746 by Gabriel Bever - Johns Hopkins University , Wiley Online Library on [30/09/2024]. See the Terms and Conditions (https://onlinelibrary.wiley.com/terms-and-conditions) on Wiley Online Library for rules of use; OA articles are governed by the applicable Creative Commons License

Structure (*x*/*y*)	*p*-value	Slope	CI	r^2	*y*-intercept
OB/OT	<0.001	0.38	0.26, 0.43	0.93	0.91
OB/TT	0.859	0.68	0.29, 0.85	0.84	1.57
CER/OB	<0.001	1.84	1.40, 2.24	0.88	−3.65
CER/OT	0.413	0.73	0.53, 0.92	0.84	−0.54

TABLE 2 Select results from analyses of covariance (ANCOVA) testing for allometry in embryonic chickens (HH19–44).

Note: Twenty-four of 29 regression slopes were allometric, of which we highlight regressions of olfactory bulb (OB) with both adjacent structures, olfactory turbinates (OT), and cerebrum (CER). Just five growth relationships, of which we highlight OB with all turbinates (TT) and CER with OT, were no different from isometry. See Data S1 for additional ANCOVA results.

Abbreviations: ANCOVA, analysis of covariance; HH, Hamburger Hamilton; OB, olfactory bulb; CER, cerebrum; OT, olfactory turbinate; TT, total turbinate.

2.2.2 | Full chicken ontogeny (HH19-Adult)

Results from developmental stages generated in the present study were amalgamated with sparser, published data from full chicken ontogeny (Table 3, Figure 7).[21] Any isometric relationship in the earlier study is also recovered as isometric here. One such relationship is between OB and olfactory turbinate ($p = 0.793$, slope = 0.65, 95% CI: 0.36, 0.8). Although the confidence interval around the null hypothesis is narrower in the present study, this relationship still is not different from isometry. This similar result under stricter conditions strongly suggests these two organs do grow in isometry with each other. All other bivariate growth relationships fell out as allometric (see also Figure 2).

3 | DISCUSSION

The present study is congruent with previous results in supporting the hypothesis that allometric growth relationships and temporal differences in developmental onset underlie morphological disparity during early nasal and brain development in chick.[21] Improved early sampling indicates differential early growth between OB and cerebrum. Cerebral volume grows episodically during these early stages but never experiences stasis; its growth even accelerates near hatching. The OB also grows episodically but does experience periods of volumetric stasis across the same developmental window. Fluctuations in OB growth rate are generally out of sync with cerebral growth, with volumetric ratios of these structures consequently fluctuating in magnitude. Periods of OB stasis seem to drive oscillations in this ratio.

Denser early sampling also allows a more precise estimate of the timing of primary OB growth. Our data show that highest rates of growth fall between HH37 and HH38, and second highest rates fall between HH31 and HH34. The most conservative interpretation of the results, given the modest sample size, is one of steady growth obscured by individual variation. The apparent reduction in OB volume from HH34 to HH35, however, was unexpected and may reflect deceleration to stasis, given that specimens at these stages are nearly equivalent in size. Vagaries of diceCT staining may impact measurement precision,[34] but staining in diceCT data of different stages (Figures 3–5) is comparable, supporting the general trends discussed herein.

Timing of associations between OB, cerebrum, and olfactory epithelium could help explain the results. First detection of the OB, at HH24, coincides with CN1-telencephalon contact. Axonal outgrowth from the nasal placode may thus induce OB growth.[16,35] The appearance of OB at HH24 is 3 days earlier than previously reported (ca. HH31).[36] Increases in OB growth rate around HH34 and HH38 coincide with other neurosensory milestones in chick. Synaptogenesis between sensory axon terminals and the main OB neurons (mitral tufted cells) begins around HH34.[36] The olfactory system becomes functional around HH38, and this event coincides

FIGURE 5 Images from diceCT data of developing brain and peripheral olfactory system from embryonic stages HH37-44 of chick *Gallus gallus*. (A, G, M, S) 3-D reconstructions of specimens at stage HH37 (A), HH38 (G), HH41 (M), and HH44 (S). Red lines indicate planes of cross-sectional images. (B, C, H, I, N, O, T, U) Cross-sectional images whose planes are illustrated in the preceding. Contrast the relatively simple hillock of olfactory turbinates (OT) with the scrolled structure of middle turbinates (MT). (D, J, P, V) Magnified left rostrolateral views of brain and peripheral olfactory system. (E, K, Q, W) Magnified left lateral views of turbinate structures. Atrial turbinates (AT) continue to develop in the lateral recess of the vestibular turbinates (VT). (F, L, R, X) Magnified rostrodorsal views of turbinate structures. AT, atrial turbinate; CN1, olfactory n.; diceCT, diffusible iodine-based contrast-enhanced microCT; HH, Hamburger Hamilton; MT, middle turbinate; OB, olfactory bulb; OT, olfactory turbinate; VT, vestibular turbinate.

10970177, 0, Downloaded from https://anatomypubs.onlinelibrary.wiley.com/doi/10.1002/dvdy.746 by Gabriel Bever - Johns Hopkins University , Wiley Online Library on [30/09/2024]. See the Terms and Conditions (https://onlinelibrary.wiley.com/terms-and-conditions) on Wiley Online Library for rules of use; OA articles are governed by the applicable Creative Commons License

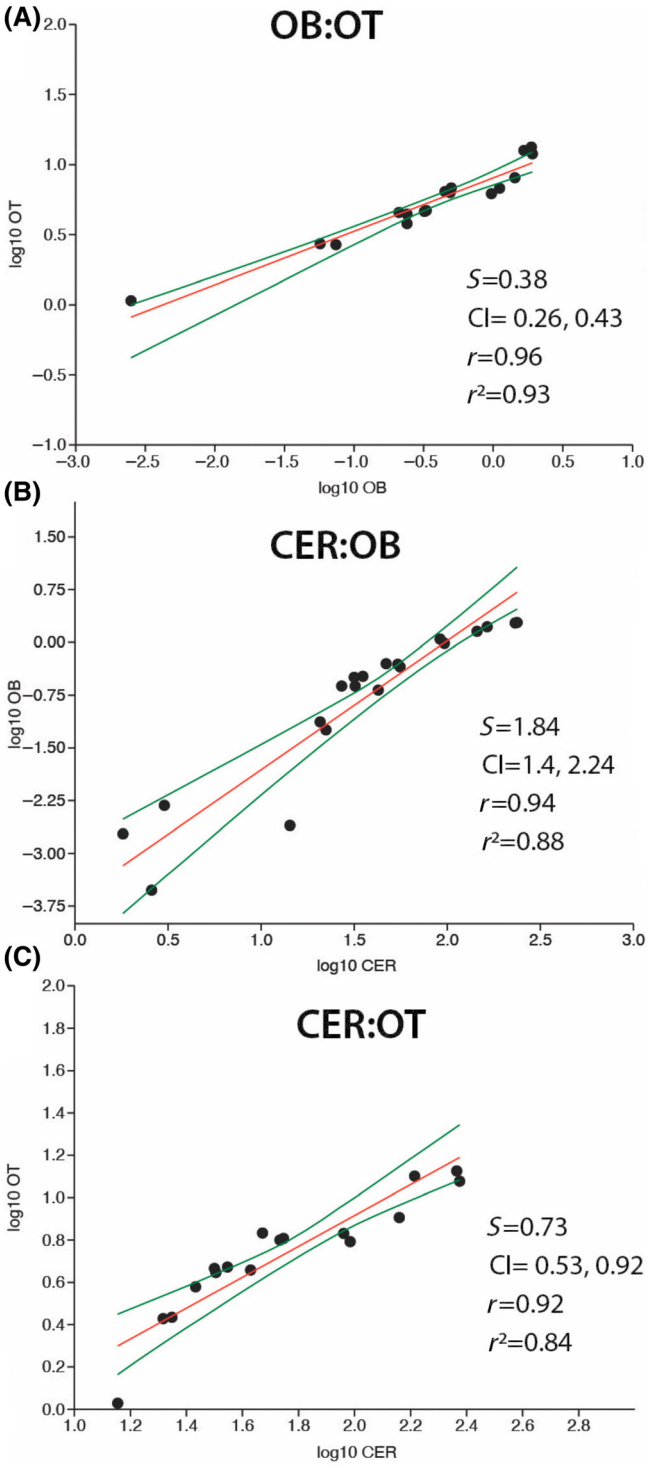

FIGURE 6 Bivariate plots of log-transformed size metrics, including embryonic data from HH19-44 with RMA line (red) and 95% confidence intervals (green). (A) Negatively allometric relationship between olfactory bulb volume (OB) and olfactory turbinate surface area (OT). (B) Positively allometric relationship between cerebrum volume (CER) and OB. (C) Isometric relationship between CER and OT. CER, cerebrum; HH, Hamburger Hamilton; OB, olfactory bulb; OT, olfactory turbinate; RMA, reduced major axis regression.

with first localization of calcium-dependent calmodulin kinase II (CaMKII) within dendrites of olfactory receptor neurons.[37] Changes in CaMKII regulation thus may affect development of olfactory epithelium and OB.

These plausible connections with our results suggest that OB growth can be partitioned into three phases correlated with olfactory developmental milestones, as follows: (1) HH24, coinciding with CN1-telencephalon contact; (2) HH34, during synaptogenesis between receptor neurons and mitral tufted cells; and (3) HH38, coinciding with initiation of signal transduction from receptor neurons to OB. That these volumetric increases correspond with neuronal development is not unexpected. All else being equal, adding neurons should equate to added volume.

One question raised by interdependent development of OB and nasal olfactory epithelium is whether similar growth patterns are found in the olfactory turbinates. Contrary to previous results,[21] the OB grows allometrically with olfactory turbinates in pre-hatch development. The OB, however, grows isometrically with middle turbinates, respiratory turbinates, and total turbinates (see Table S4). The isometry recovered between OB and total turbinates makes sense considering that, relative to OB, the olfactory and respiratory turbinates scale with similar levels of negative and positive allometry, respectively (i. e., canceling out).

Our study reveals that pre-hatching OB growth outpaces that of the olfactory turbinates, whereas these structures grow isometrically when post-hatch ontogeny is also considered. In contrast, the addition of post-hatching values results in the loss of isometry between the olfactory turbinate and other brain regions. These changes likely arise from two sources: first, the intimate connection between OB and olfactory epithelium, and second, the postnatal pruning of transitory olfactory projections from OB to the rest of the brain. OB volume is associated with neuronal regeneration and signal transduction from the olfactory epithelium throughout life span.[38] There is a one-to-one axonal connection from each olfactory receptor neuron to glomeruli in the OB.[13,39] The maintenance of these connections could explain isometry between OB and olfactory turbinate in post-hatch data. Transitory olfactory projections from OB to brain are dense during pre-hatch development but are pruned after hatching. This pruning presumably attenuates the neuronal connection between OB and brain. As growth of the cerebrum and whole brain outpaces that of the OB—concurrent with pruning—the morphometric relationship between OB and brain breaks down. At that point in time, the rostral connection between OB and olfactory epithelium, which is regenerating (i. e., not

10970177, 0, Downloaded from https://anatomypubs.onlinelibrary.wiley.com/doi/10.1002/dvdy.746 by Gabriel Bever - Johns Hopkins University , Wiley Online Library on [30/09/2024]. See the Terms and Conditions (https://onlinelibrary.wiley.com/terms-and-conditions) on Wiley Online Library for rules of use; OA articles are governed by the applicable Creative Commons License

Structure (*x*/*y*)	*p*-value	Slope	CI	r^2	*y*-intercept
OB/OT	0.793	0.65	0.36, 0.80	0.78	1.09
CER/OB	<0.001	1.37	1.08, 1.70	0.85	−3.08
CER/OT	0.026	0.76	0.69, 0.86	0.92	−0.63

TABLE 3 Select results from analysis of covariance (ANCOVA) testing for allometry across full ontogeny (HH19-adult).

Note: Eleven of 12 regression slopes were allometric, of which we highlight cerebrum (CER) with olfactory bulb (OB) and CER with olfactory turbinates (OT). Just one growth relationship (OB/OT) was no different from isometry. See Data S1 for additional ANCOVA results.
Abbreviations: ANCOVA, analysis of covariance; HH, Hamburger Hamilton; CER, cerebrum; OB, olfactory bulb; OT, olfactory turbinate.

being pruned), becomes reflected quantitatively in an isometric growth relationship between OB and olfactory turbinate. This isometric relationship was recovered in more coarsely sampled postnatal ontogeny.[21]

4 | CONCLUSIONS

These early developmental data paint a picture of complex growth trajectories of the OB and related olfactory structures. Multiple periods of accelerated volumetric growth in the OB are unsurprising, considering the tempo of its neuronal establishment and subsequent synaptogenesis. Isometry between the olfactory turbinate and brain structures other than the OB (i. e., cerebrum and brain-minus-telencephalon) are unexpected given previous work, but results from the present study make sense considering the pre-hatch transience and later manifestation of olfactory neural connections. These findings emphasize the importance of densely sampling a narrow window of development when attempting to understand the dynamics through which disparate morphologies form. These data suggest that caudal olfactory projections into the telencephalon and diencephalon during embryogenesis play a role in neuronal tradeoffs impacting the size and morphology of the primary olfactory structures, including the olfactory turbinates. Maturation of this sensory system is thus more complex than previously appreciated. In evaluating olfactory and turbinate morphogenesis in the larger context of cranial neurosensory development in a classic model organism, our new data also are a foundation for comparative work and, thereby, examination of evolutionary factors that act on this neurosensory system.

5 | EXPERIMENTAL PROCEDURES

5.1 | Specimens

A developmental series of *Gallus gallus domesticus* (white leghorn chicken) were incubated to target stages encompassing the main window of olfactory and nasal development. As early stages were absent in previous work,[21] a sampling was adopted that targeted days 3–18 of embryonic development with increased sampling during the highest periods of growth of this system. This time period encompasses the earliest reported developmental growth of the olfactory system in chick.[21]

Thirty-six premium specific-pathogen-free (SPF) fertile eggs from flock L176 were procured from Charles River Laboratories in North Franklin, CT, USA. See Data S1 for more details on shipment and handling of specimens. Eggs were incubated at Johns Hopkins School of Medicine for predetermined periods of time. Embryos were harvested on days 3, 4, 6, 7, 8, 10, 11 of incubation. These data were supplemented with previous data from days 5, 9, 12, 15, and 18.[21] Since the supplier lists its expectations for eggs as 85%–90% viability and 85% fertility, we incubated five eggs per predetermined time point to improve our chances of having two viable specimens at each time point. Embryos were staged using the Hamburger Hamilton (HH) system on each day they were harvested: HH 19 (day 3), HH 24 (day 4), HH 26–27 (day 5), HH 29 (day 6), HH 31 (day 7), HH 34 (day 8), HH 35 (day 9), HH 36 (day 10), HH 37 (day 11), HH 38 (day 12), HH 41 (day 15), and HH 44 (day 18).

5.2 | Incubation and Processing

We incubated eggs at 99.4 °F-99.8 °F and between 55% and 60% humidity using a Genesis Hova-Bator 1602 N and a Hova-Bator Genesis 1588. See Data S1 for additional details on incubation. At our target time-points, embryos were extracted, weighed, and humanely euthanized.[40] Specimens were then washed with and suspended in phosphate-buffered saline (PBS). Photographs were taken with a Nikon SMZ1270 Stereoscopic Microscope and standard measurements (i. e., length, width) recorded. Specimens were then transferred to 10 or 50 mL standing centrifuge tubes for small or large embryos, respectively.

10970177, 0, Downloaded from https://anatomypubs.onlinelibrary.wiley.com/doi/10.1002/dvdy.746 by Gabriel Bever - Johns Hopkins University , Wiley Online Library on [30/09/2024]. See the Terms and Conditions (https://onlinelibrary.wiley.com/terms-and-conditions) on Wiley Online Library for rules of use; OA articles are governed by the applicable Creative Commons License

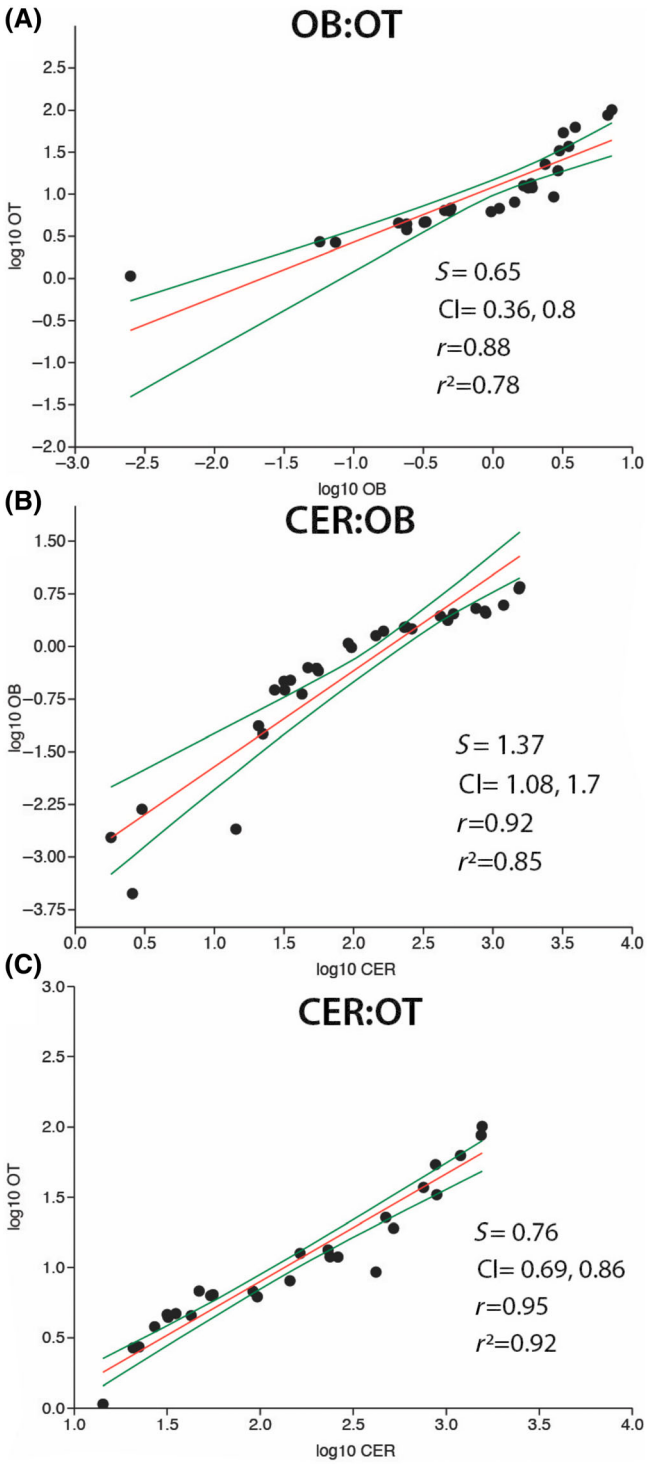

FIGURE 7 Bivariate plots of log-transformed size metrics, including data amalgamated from this study (HH19-Adult) and previous work,[21] with RMA line (red) and 95% confidence intervals (green). (A) Isometric relationship between olfactory bulb volume (OB) and olfactory turbinate surface area (OT). (B) Positively allometric relationship between cerebrum volume (CER) and OB. (C) Positively allometric relationship between CER and OT. CER, cerebrum; HH, Hamburger Hamilton; OB, olfactory bulb; OT, olfactory turbinate; RMA, reduced major axis regression.

5.3 | Hydrogel STABILITY procedure

Embryos were immersed in hydrogel to stabilize tissues. We immersed embryos in a gel precursor that was in a liquid state (solution of 38% Acrylamide and 2% Bis-acrylamide by Amresco). The solution was heated to activate polymerization, during which embryonic tissues experience molecular "cross-linking" with the hydrogel. This process is analogous to plastination but leaves the specimen receptive to differential staining. Our protocol is a combination of published approaches.[41–43] See Data S1 for step-by-step instructions that we used to create the hydrogel.

5.4 | Iodine staining and agarose gel

We applied Lugol's iodine solution (iodine potassium iodide, aqueous) as a contrast stain in a diffusible-iodine contrast-enhanced CT-scanning, or diceCT protocol.[21,34,41,44,45] Different concentrations of Lugol's iodine solution were used depending on the age of the specimen (Data S1). Too high a concentration of Lugol's iodine may damage early developing tissues that contain a lot of water, including by differentially shrinking brain regions.[41,43,46] We employed the STABILITY (hydrogel) protocol, outlined in the preceding section, which effectively eliminates the risk of shrinkage or at worst mitigates it.

To increase the rate of uptake and prevent further polymerization, hydrogel specimens were stained at 4°C. All specimens were initially stained for a duration of 14 days, with fresh iodine being swapped out every few days. Specimens were also agitated periodically on a VEVOR Orbital Rotator Shaker to diffuse iodine more evenly. A solution of 0.16% Lugol's iodine (0.16 g I_2+ 0.33 g K + 99.8 mL de-ionized H_20, or 0.50% total solute concentration) was used to stain specimens harvested on day 3. Specimens harvested on day 4 were stained with a 0.33% Lugol's iodine solution (1% total solute). Specimens harvested on days 6–8 were all stained with a 1% Lugol's iodine solution (3% total solute). Some specimens required additional time, of up to two more weeks, and higher concentrations of Lugol's iodine to stain sufficiently for CT scanning (see Data S1 for details).

A 1% clear agar solution was added to the centrifuge tubes to suspend and protect specimens during scanning. A thin layer of iodine was added to the top agar surface to act as an antimicrobial and prevent unintended bacterial growth.

5.5 | MicroCT Scanning

Embryos were scanned at Johns Hopkins University using RX Solutions Micro Computed Tomography.

10970177, 0, Downloaded from https://anatomypubs.onlinelibrary.wiley.com/doi/10.1002/dvdy.746 by Gabriel Bever - Johns Hopkins University , Wiley Online Library on [30/09/2024]. See the Terms and Conditions (https://onlinelibrary.wiley.com/terms-and-conditions) on Wiley Online Library for rules of use; OA articles are governed by the applicable Creative Commons License

Three-dimensional datasets were acquired for each specimen with a high-power sealed microfocus 150 kV x-ray source and an open nanofocus 160 kV x-ray source, both with a flat panel detector. Samples (i. e., tubes with embryos in them) were secured to a 360° rotation bed, and each tube was scanned separately in custom, tightly fit sample holders. This approach, in addition to suspension in agar, meant most specimens experienced minimal movement during acquisition, which otherwise would require re-scanning. Any specimens that did experience movement during acquisition were refastened to the scan bed before re-scanning with the same scan parameters as the first attempt. Additional details on securing specimens to the scan bed and scanner settings may be referred to in Data S1 (Supporting Table 2).

5.6 | Segmentation

3-D image stacks from μCT data reconstructions were examined and segmented in Amira v 6.3 (Thermo Fisher Scientific). Before segmentation, image stacks were run through a contrast-limited adaptive histogram equalization (CLAHE) procedure in Fiji (ImageJ).[47] The CLAHE procedure enhances local contrast across entire images and image stacks, applying multiple equalizations within partitions of an image, and corrects for areas that are overly dark or bright white.[21,47,48] Nasal and brain anatomy were isolated and segmented following established protocols.[21] Identification of structures was aided by differential uptake of iodine stains into sensory versus nonsensory tissue (i. e., olfactory epithelia appear white in scans when compared with respiratory epithelia). The full path of CN1 was not clear in all specimens, so CN1 is only described in terms of gross morphological maturation across the series and is not included in quantitative analyses.

Due to the amorphous nature of embryos and progressive tissue differentiation across developmental stages, multiple tools were used for segmentation and no two CT datasets required identical processing. Automated tools, including thresholding and algorithms for edge detection, worked in some late-stage embryos. However, for most of the sample, the difference in radiodensity between focal tissues and surrounding mesenchyme was too subtle for the automated tools to detect (e. g., turbinates and nasal plug). Anatomical boundaries were instead primarily identified by sight and segmented by hand with the paintbrush and lasso tools. A semi-automated process, interpolation, was used to increase the efficiency of segmentation. Every third slice (for the smaller turbinate structures) or every 5–10 slices (for the larger brains), segmentation was carried out by hand. An algorithm preprogrammed in Amira then interpolated between these segmented slices, producing a 3-D volume. We then manually edited the resulting 3-D volume to correct any errors introduced during the interpolation process. Surface areas (turbinate structures) and volumes (brain structures) were measured using volume and surface area measurement tools in Amira (Table 4).

5.7 | Analyses

To evaluate raw growth, volumetric and surface area measurements of each structure were plotted against time in days. Best-fit logistic and exponential growth curves were estimated and visualized using the "fit_spline" and "fit_growthmodel" commands in the R-package {growthrates}.[49] Ratios of olfactory-related structures were also plotted against age to visualize relative growth between structures. Plots were created by averaging the volumes and surface areas at each stage with two representative specimens. Growth rates were calculated (Table 1) by dividing change in size over time $(y2-y1)/(t2-t1)$.[50] Additionally, percent increases were calculated (Table 1) by dividing change in size by initial size of the focal structure $(y2-y1)/y1$.[50,51] Pairwise comparisons of volumes and surface areas were used to assess relative scaling differences between individual structures. Brain regions were assessed against each other and against whole brain volumes with the region of interest subtracted. For example, when evaluating the OB against the whole brain, OB volume is subtracted from the whole brain volume (brain-OB). In addition, brain regions were compared to individual turbinates, grouped respiratory turbinates, and combined turbinates. Turbinates were assessed against other discrete turbinate types and against grouped respiratory turbinates.

Measured surface areas and volumes were evaluated using a bivariate Model II regression analysis (Tables 2, 3; Figures 6 and 7; Figures S1 and S2). Reduced major axis regression (RMA) was used to account for error in both predictor and response variables.[52,53] Analyses of covariance (ANCOVA) were then performed to assess whether observed RMA slopes differed from isometry (H_A) or were indistinguishable from isometry (H_0). A slope of 0.67 is isometric when regressing surface area (i. e., a two-dimensional measurement) with volume (i. e., a three-dimensional measurement), whereas a slope of 1.0 is isometric when variables share dimensions (e. g., volume to volume).

After evaluating the ontogenetic series collected for the present study, which focused on pre-hatch development and included HH19–HH44, these data were then amalgamated with post-hatch data (Day 1-Adult).[21]

10970177, 0, Downloaded from https://anatomypubs.onlinelibrary.wiley.com/doi/10.1002/dvdy.746 by Gabriel Bever - Johns Hopkins University , Wiley Online Library on [30/09/2024]. See the Terms and Conditions (https://onlinelibrary.wiley.com/terms-and-conditions) on Wiley Online Library for rules of use; OA articles are governed by the applicable Creative Commons License

TABLE 4 Surface area (mm^2) and volume (mm^3) of olfactory and brain structures.

Specimen	HH stage	OB (mm^3)	CER (mm^3)	Tot brain (mm^3)	Olf turb (mm^2)	Mid turb (mm^2)	Vest turb (mm^2)	Atrial turb (mm^2)	Tot turb (mm^2)
3a	19	—	0.254	1.33	—	—	—	—	—
3b	19	—	0.176	0.685	—	—	—	—	—
4a	24	0.001	1.81	7.32	—	—	—	—	—
5a	26	0.0003	2.58	6.94	—	—	—	—	—
5b	27	0.004	3.02	11.3	—	—	—	—	—
6a	29	0.002	14.2	46.1	1.07	0.830	—	—	1.90
7a	31	0.074	20.7	71.3	2.68	1.17	0.570	—	4.42
7b	31	0.057	22.3	69.0	2.72	2.05	0.810	—	5.58
8a	34	0.320	31.6	92.6	4.63	3.18	1.12	—	8.93
8b	34	0.240	27.0	87.0	3.79	3.86	0.890	—	8.54
9a	35	0.210	42.5	132	4.55	3.54	1.47	0.050	9.61
9b	35	0.240	31.9	111	4.43	4.62	1.72	0.200	10.9
10a	36	0.499	46.9	147	6.81	4.87	4.66	1.19	17.5
10b	36	0.330	35.1	114	4.70	4.22	4.48	0.670	14.0
11a	37	0.490	54.1	165	6.31	9.59	7.46	0.980	24.3
11b	37	0.450	55.7	168	6.42	8.64	7.74	0.950	23.7
12a	38	0.970	96.4	227	6.20	14.5	9.80	1.96	32.4
12b	38	1.11	91.4	213	6.78	12.6	7.74	1.19	28.3
15a	41	1.43	144	339	8.06	21.1	14.0	4.49	47.6
15b	41	1.66	163	395	12.6	26.2	18.8	6.32	63.9
18a	44	1.91	237	579	11.9	37.5	39.1	13.1	101
18b	44	1.88	231	594	13.3	53.7	44.2	16.2	127

Abbreviation: CER, cerebrum; HH, Hamburger Hamilton; Mid, middle; OB, olfactory bulb; Tot, total; turb, turbinates; Vest, vestibular.

A second analysis with the amalgamated dataset, using the same regression and ANCOVA approach, was carried out to compare the effects of denser sampling (relative to the earlier study[21]) of developmental stages within the context of full ontogeny. All data were log-transformed prior to analyses and were processed using (S)MATR and PAST version 4.0.[54,55]

ACKNOWLEDGMENTS

The authors have no conflict of interest to declare. This study was supported through funding from NSF DEB-1947001 (to GSB). The authors thank Aki Watanabe, Amy Balanoff, Siobhán Cooke, Tim Smith, and D. J. Morgan for constructive dialogue, at various points of the project, that improved the article. The authors also thank the reviewers for their helpful comments, which improved the article.

FUNDING INFORMATION

National Science Foundation Division of Environmental Biology, DEB-1947001.

CONFLICT OF INTEREST STATEMENT

The authors declare no conflicts of interest.

DATA AVAILABILITY STATEMENT

A spreadsheet of raw measurements from the sample is included in the main text as Table 4.

ORCID

Donald G. Cerio https://orcid.org/0000-0002-7517-5791

REFERENCES

1. Schlosser G. Induction and specification of cranial placodes. *Dev Biol*. 2006;294(2):303-351. doi:10.1016/j.ydbio.2006.03.009
2. Szabo-Rogers HL, Geetha-Loganathan P, Whiting CJ, Nimmagadda S, Fu K, Richman JM. Novel skeletogenic patterning roles for the olfactory pit. *Development*. 2009;136(2):219-229. doi:10.1242/dev.023978
3. Steventon B, Mayor R, Streit A. Neural crest and placode interaction during the development of the cranial sensory system. *Dev Biol*. 2014;389(1):28-38. doi:10.1016/j.ydbio.2014.01.021
4. Leibovici M, Lapointe F, Aletta P, Ayer-Le LC. Avian olfactory receptors: differentiation of olfactory neurons under normal

10970177, 0, Downloaded from https://anatomypubs.onlinelibrary.wiley.com/doi/10.1002/dvdy.746 by Gabriel Bever - Johns Hopkins University , Wiley Online Library on [30/09/2024]. See the Terms and Conditions (https://onlinelibrary.wiley.com/terms-and-conditions) on Wiley Online Library for rules of use; OA articles are governed by the applicable Creative Commons License

and experimental conditions. *Dev Biol*. 1996;175(1):118-131. doi:10.1006/dbio.1996.0100
5. Marcucio RS, Young NM, Hu D, Hallgrimsson B. Mechanisms that underlie co-variation of the brain and face. *Genesis*. 2011;49(4):177-189. doi:10.1002/dvg.20710
6. Griffin JN, Compagnucci C, Hu D, et al. Fgf8 dosage determines midfacial integration and polarity within the nasal and optic capsules. *Dev Biol*. 2013;374(1):185-197. doi:10.1016/j.ydbio.2012.11.014
7. Jidigam VK, Gunhaga L. Development of cranial placodes: insights from studies in chick. *Dev Growth Differ*. 2013;55(1):79-95. doi:10.1111/dgd.12027
8. Abramyan J, Richman JM. Craniofacial development: discoveries made in the chicken embryo. *Int J Dev Biol*. 2018;62(1-2-3):97-107. doi:10.1387/ijdb.170321ja
9. Kaucka M, Petersen J, Tesarova M, et al. Signals from the brain and olfactory epithelium control shaping of the mammalian nasal capsule cartilage. *Elife*. 2018;7:e34465. doi:10.7554/eLife.34465
10. Yang LM, Ornitz DM. Sculpting the skull through neurosensory epithelial-mesenchymal signaling. *Dev Dyn*. 2019;248(1):88-97. doi:10.1002/dvdy.24664
11. Minkoff R, Kuntz AJ. Cell proliferation during morphogenetic change; analysis of frontonasal morphogenesis in the chick embryo employing DNA labeling indices. *J Embryol Exp Morphol*. 1977;40:101-113. doi:10.1242/dev.40.1.101
12. Butler AB, Hodos W. *Comparative Vertebrate Neuroanatomy: Evolution and Adaptation*. Second ed. Wiley-Interscience; 2005.
13. Serizawa S, Miyamichi K, Sakano H. One neuron-one receptor rule in the mouse olfactory system. *Trends Genet*. 2004;20(12):648-653. doi:10.1016/j.tig.2004.09.006
14. Lancet D. Vertebrate olfactory reception. *Annu Rev Neurosci*. 1986;9:329-355. doi:10.1146/annurev.ne.09.030186.001553
15. Buck L, Axel R. A novel multigene family may encode odorant receptors: a molecular basis for odor recognition. *Cell*. 1991;65(1):175-187. doi:10.1016/0092-8674(91)90418-x
16. Gong Q, Shipley MT. Evidence that pioneer olfactory axons regulate telencephalon cell cycle kinetics to induce the formation of the olfactory bulb. *Neuron*. 1995;14(1):91-101. doi:10.1016/0896-6273(95)90243-0
17. Gould SJ. Allometry and size in ontogeny and phylogeny. *Biol Rev Camb Philos Soc*. 1966;41(4):587-640. doi:10.1111/j.1469-185x.1966.tb01624.x
18. Gould SJ. *Ontogeny and Phylogeny*. The Belknap Press of Harvard University Press; 1977.
19. Klingenberg CP. Heterochrony and allometry: the analysis of evolutionary change in ontogeny. *Biol Rev Camb Philos Soc*. 1998;73(1):79-123. doi:10.1017/s000632319800512x
20. Hallgrímsson B, Jamniczky H, Young NM, et al. Deciphering the palimpsest: studying the relationship between morphological integration and phenotypic covariation. *Evol Biol*. 2009;36(4):355-376. doi:10.1007/s11692-009-9076-5
21. Hogan AVC, Watanabe A, Balanoff AM, Bever GS. Comparative growth in the olfactory system of the developing chick with considerations for evolutionary studies. *J Anat*. 2020;237(2):225-240. doi:10.1111/joa.13197
22. Klingenberg CP, Marugán-Lobón J. Evolutionary covariation in geometric morphometric data: analyzing integration, modularity, and allometry in a phylogenetic context. *Syst Biol*. 2013;62(4):591-610. doi:10.1093/sysbio/syt025
23. Niimura Y, Nei M. Extensive gains and losses of olfactory receptor genes in mammalian evolution. *PLoS One*. 2007;2(8):e708. doi:10.1371/journal.pone.0000708
24. Steiger SS, Fidler AE, Valcu M, Kempenaers B. Avian olfactory receptor gene repertoires: evidence for a well-developed sense of smell in birds? *Proc R Soc B*. 2008;275(1649):2309-2317. doi:10.1098/rspb.2008.0607
25. Hughes GM, Finarelli JA. Olfactory receptor repertoire size in dinosaurs. *Proc R Soc B*. 1904;2019(286):20190909. doi:10.1098/rspb.2019.0909
26. Shykind BM. Regulation of odorant receptors: one allele at a time. *Hum Mol Genet*. 2005;14(suppl_1):R33-R39. doi:10.1093/hmg/ddi105
27. Green PA, Van Valkenburgh B, Pang B, Bird D, Rowe T, Curtis A. Respiratory and olfactory turbinal size in canid and arctoid carnivorans. *J Anat*. 2012;221(6):609-621. doi:10.1111/j.1469-7580.2012.01570.x
28. Van Valkenburgh B, Smith TD, Craven BA. Tour of a labyrinth: exploring the vertebrate nose. *Anat Rec*. 2014;297(11):1975-1984. doi:10.1002/ar.23021
29. Yang LM, Huh SH, Ornitz DM. FGF20-expressing, Wnt-responsive olfactory epithelial progenitors regulate underlying turbinate growth to optimize surface area. *Dev Cell*. 2018;46(5):564-580.e5. doi:10.1016/j.devcel.2018.07.010
30. Eisthen HL. Why are olfactory systems of different animals so similar? *Brain Behav Evol*. 2002;59(5–6):273-293. doi:10.1159/000063564
31. Alrajeh M, Vavrusova Z, Creuzet SE. *Deciphering the Neural Crest Contribution to Cephalic Development with Avian Embryos. In: Schwarz Q, Wiszniak S, Eds. Neural Crest Cells. Vol 1976. Methods in Molecular Biology*. Springer New York; 2019:55-70. doi:10.1007/978-1-4939-9412-0_5
32. Albawaneh Z, Ali R, Abramyan J. Novel insights into the development of the avian nasal cavity. *Anat Rec*. 2021;304(2):247-257. doi:10.1002/ar.24349
33. Striedter GF, Charvet CJ. Developmental origins of species differences in telencephalon and tectum size: morphometric comparisons between a parakeet (*Melopsittacus undulatus*) and a quail (*Colinus virgianus*). *J Comp Neurol*. 2008;507(5):1663-1675. doi:10.1002/cne.21640
34. Gignac PM, Kley NJ, Clarke JA, et al. Diffusible iodine-based contrast-enhanced computed tomography (diceCT): an emerging tool for rapid, high-resolution, 3-D imaging of metazoan soft tissues. *J Anat*. 2016;228(6):889-909. doi:10.1111/joa.12449
35. Van Campenhout E. Le développement du système nerveux cranien chez le poulet. *Arch Biol*. 1937;48:611-666.
36. Ayer-Le Lièvre C, Lapointe F, Leibovici M. Avian olfactory neurogenesis. *Biol Cell*. 1995;84(1–2):25-34. doi:10.1016/0248-4900(96)81315-3
37. Lalloué FL, Ayer-Le Lièvre CS, Sicard G. Analysis of the functional maturation of olfactory neurons in chicks before and after birth. *Chem Senses*. 2003;28(8):729-737. doi:10.1093/chemse/bjg055
38. Brann JH, Firestein SJ. A lifetime of neurogenesis in the olfactory system. *Front Neurosci*. 2014;8:182. doi:10.3389/fnins.2014.00182
39. Rodriguez I. Singular expression of olfactory receptor genes. *Cell*. 2013;155(2):274-277. doi:10.1016/j.cell.2013.09.032

10970177, 0, Downloaded from https://anatomypubs.onlinelibrary.wiley.com/doi/10.1002/dvdy.746 by Gabriel Bever - Johns Hopkins University , Wiley Online Library on [30/09/2024]. See the Terms and Conditions (https://onlinelibrary.wiley.com/terms-and-conditions) on Wiley Online Library for rules of use; OA articles are governed by the applicable Creative Commons License

40. Leary S, Underwood W, Anthony R, et al. *AVMA Guidelines for the Euthanasia of Animals*. American Veterinary Medical Association; 2020.
41. Wong MD, Spring S, Henkelman RM. Structural Stabilization of Tissue for Embryo Phenotyping Using Micro-CT with Iodine Staining. *PLoS ONE*. 2013;8(12):e84321. doi:10.1371/journal.pone.0084321
42. Carlisle A, Weisbecker V. A modified STABILITY protocol for accurate retrieval of soft-tissue data from micro-CT scans of IKI-stained specimens. 2016. Published August 9, https://dicect.com/2016/08/09/stability/.
43. Carlisle A, Selwood L, Hinds LA, et al. Testing hypotheses of developmental constraints on mammalian brain partition evolution, using marsupials. *Sci Rep*. 2017;7(1):4241. doi:10.1038/s41598-017-02726-9
44. Metscher BD. MicroCT for developmental biology: a versatile tool for high-contrast 3D imaging at histological resolutions. *Dev Dyn*. 2009;238(3):632-640. doi:10.1002/dvdy.21857
45. Gignac PM, Kley NJ. Iodine-enhanced micro-CT imaging: methodological refinements for the study of the soft-tissue anatomy of post-embryonic vertebrates. *J Exp Zool B Mol Dev Evol*. 2014;322(3):166-176. doi:10.1002/jez.b.22561
46. Degenhardt K, Wright AC, Horng D, Padmanabhan A, Epstein JA. Rapid 3D phenotyping of cardiovascular development in mouse embryos by micro-CT with iodine staining. *Circ Cardiovasc Imaging*. 2010;3(3):314-322. doi:10.1161/CIRCIMAGING.109.918482
47. Zuiderveld K. Contrast limited adaptive histogram equalization. *Graphics Gems*. Elsevier; 1994:474-485. doi:10.1016/B978-0-12-336156-1.50061-6
48. Mayya V, SSK, Kulkarni U, Surya DK, Acharya UR. An empirical study of preprocessing techniques with convolutional neural networks for accurate detection of chronic ocular diseases using fundus images. *Appl Intell*. 2023;53(2):1548-1566. doi:10.1007/s10489-022-03490-8
49. Petzoldt T. Growthrates: estimate growth rates from experimental data. 2022. https://CRAN.R-project.org/package=growthrates.
50. Huxley J. *Problems of Relative Growth*. 2d ed. Dover; 1972.
51. Desmond ME, O'Rahilly R. The growth of the human brain during the embryonic period proper: 1. Linear axes. *Anat Embryol*. 1981;162(2):137-151. doi:10.1007/BF00306486
52. Warton DI, Wright IJ, Falster DS, Westoby M. Bivariate line-fitting methods for allometry. *Biol Rev Camb Philos Soc*. 2006;81(2):259-291. doi:10.1017/S1464793106007007
53. Sokal RR, Rohlf FJ. *Biometry: the Principles and Practice of Statistics in Biological Research*. 3rd ed. Freeman; 2010.
54. Falster DS, Warton DI, Wright IJ. SMATR: standardised major axis tests and routines. 2006. Published Online, https://github.com/dfalster/smatr
55. Hammer Ø, Harper DAT, Ryan PD. PAST: paleontological statistics software package for education and data analysis. *Palaeontol Electron*. 2001;4(1):9. https://palaeo-electronica.org/2001_1/past/issue1_01.htm

SUPPORTING INFORMATION

Additional supporting information can be found online in the Supporting Information section at the end of this article.

How to cite this article: Hogan AVC, Cerio DG, Bever GS. Patterns of early embryogenesis and growth in the olfactory system of chick (*Gallus gallus domesticus*) based on iodine-enhanced micro-computed tomography. *Developmental Dynamics*. 2024;1-17. doi:10.1002/dvdy.746

10970177, 0, Downloaded from https://anatomypubs.onlinelibrary.wiley.com/doi/10.1002/dvdy.746 by Gabriel Bever - Johns Hopkins University , Wiley Online Library on [30/09/2024]. See the Terms and Conditions (https://onlinelibrary.wiley.com/terms-and-conditions) on Wiley Online Library for rules of use; OA articles are governed by the applicable Creative Commons License